

## Promoting effect of SnO<sub>x</sub> on selective conversion of cellulose to polyols over bimetallic Pt–SnO<sub>x</sub>/Al<sub>2</sub>O<sub>3</sub> catalysts†

Cite this: *Green Chem.*, 2013, **15**, 116

Tianyin Deng and Haichao Liu\*

Cellulose is the most abundant source of biomass in nature, and its selective conversion into polyols provides a viable route towards the sustainable synthesis of fuels and chemicals. Here, we report the marked change in the distribution of polyols in the cellulose reaction with the Sn/Pt atomic ratios in a wide range of 0.1–3.8 on the SnO<sub>x</sub>-modified Pt/Al<sub>2</sub>O<sub>3</sub> catalysts. Such a change was found to be closely related to the effects of the Sn/Pt ratios on the activity for the hydrogenation of glucose and other C<sub>6</sub> sugar intermediates involved in the cellulose reaction as well as to the notable activity of the segregated SnO<sub>x</sub> species for the selective degradation of the sugar intermediates on the Pt–SnO<sub>x</sub>/Al<sub>2</sub>O<sub>3</sub> catalysts. At lower Sn/Pt ratios of 0.1–1.0, there existed electron transfer from the SnO<sub>x</sub> species to the Pt sites and strong interaction between the catalysts, as characterized by temperature-programmed reduction in H<sub>2</sub> and infrared spectroscopy for CO adsorption, which led to their superior hydrogenation activity (per exposed Pt atom), and in-parallel higher selectivity to hexitols (e.g. sorbitol) in the cellulose reaction, as compared to Pt/Al<sub>2</sub>O<sub>3</sub>. The hexitol selectivity reached the greatest value of 82.7% at the Sn/Pt ratio of 0.5, nearly two times that of Pt/Al<sub>2</sub>O<sub>3</sub> at similar cellulose conversions (~20%). As the Sn/Pt ratios exceeded 1.5, the Pt–SnO<sub>x</sub>/Al<sub>2</sub>O<sub>3</sub> catalysts exhibited inferior hydrogenation activity (per exposed Pt atom), due to the formation of the crystalline Pt–Sn alloy, which led to the preferential conversion of cellulose to C<sub>2</sub> and especially C<sub>3</sub> products (e.g. acetol) over hexitols, most likely involving the isomerization of glucose to fructose and retro-aldol condensation of these sugars on the segregated SnO<sub>x</sub> species, apparently in the form of Sn(OH)<sub>2</sub>. These findings clearly demonstrate the feasibility for rational control of the cellulose conversion into the target polyols (e.g. acetol or propylene glycol), for example, by the design of efficient catalysts based on the catalytic functions of the SnO<sub>x</sub> species with tunable hydrogenation activity.

Received 13th July 2012,  
Accepted 28th September 2012

DOI: 10.1039/c2gc36088h

[www.rsc.org/greenchem](http://www.rsc.org/greenchem)

### 1 Introduction

Catalytic conversion of cellulose to polyols has attracted great attention as one of the most viable primary routes for cellulose utilization because of the versatile uses of polyols in the synthesis of fuels and value-added chemicals.<sup>1–7</sup> This conversion route traditionally involves the use of mineral acids for cellulose hydrolysis to sugars, which are subsequently hydrogenated to polyols on metal-based catalysts.<sup>6,8,9</sup> Since the pioneering work on Pt/Al<sub>2</sub>O<sub>3</sub> in water and Ru nanoclusters in an ionic liquid,<sup>10,11</sup> recent studies on this cellulose reaction have been dedicated to the development of greener approaches

to avoid the use of mineral acids and to improve polyol productivity.

Fukuoka and Dhepe reported the direct conversion of cellulose into hexitols (*i.e.* sorbitol and mannitol) in a 31% yield at 463 K on Pt/Al<sub>2</sub>O<sub>3</sub> in the absence of mineral acids.<sup>10</sup> By taking advantage of the unique properties of water under near-critical conditions, Luo *et al.* obtained a ~40% yield of hexitols on Ru/C in combination with the hydrolysis role of H<sup>+</sup> ions reversibly formed from hot water at 513 K.<sup>12</sup> Further studies on different hydrogenation catalysts led to improved yields.<sup>13–15</sup> For example, Pang *et al.* achieved a 59.8% yield of hexitols using a mesoporous carbon supported Ni–Rh catalyst;<sup>13</sup> Sels and co-workers reported a >90% yield of hexitols at a 100% conversion of ball-milled cellulose on bifunctional Ru/H-USY catalyst in the presence of a trace amount of HCl, and even the quantitative conversion of ball-milled cellulose into hexitols on Ru/C together with heteropolyacids.<sup>14b,c</sup> More noticeably, Zhang and co-workers found that cellulose can even be converted directly to ethylene glycol on Ni–W<sub>2</sub>C/C.<sup>16</sup> These results demonstrate

Beijing National Laboratory for Molecular Sciences, College of Chemistry and Molecular Engineering, Peking University, Beijing 100871, China.

E-mail: [hcliu@pku.edu.cn](mailto:hcliu@pku.edu.cn); Fax: +86-10-6275-4031

†Electronic supplementary information (ESI) available. See DOI: 10.1039/c2gc36088h

that the polyol selectivities are strongly dependent on the properties of the hydrogenation catalysts, which accordingly influence the relative rates between the competitive hydrogenation of the sugar intermediates and their degradation. Therefore, it is necessary to further understand the underlying reasons for such a dependence in order to design more efficient catalysts towards the controllable conversion of cellulose to polyols.

Compared to monometallic catalysts, bimetallic catalysts frequently exhibit superior activity and selectivity in many reactions. Concerning the aforementioned Pt/Al<sub>2</sub>O<sub>3</sub> catalyst, its modification with SnO<sub>x</sub> as an example leads to wide applications in industry.<sup>17–19</sup> Extensive studies on the SnO<sub>x</sub>-modified Pt/Al<sub>2</sub>O<sub>3</sub> (Pt–SnO<sub>x</sub>/Al<sub>2</sub>O<sub>3</sub>) catalysts have revealed the drastically electronic and geometric effects of SnO<sub>x</sub> on the catalytic properties of the Pt sites.<sup>20,21</sup> Moreover, the presence of SnO<sub>x</sub> as a Lewis acid in the Pt catalysts can largely improve the hydrogenation of unsaturated aldehydes (*e.g.* citral, crotonaldehyde and carvone) *via* its close interaction with the carbonyl groups, to form desirable products of unsaturated alcohols.<sup>19,22–24</sup> Therefore, we herein study the Pt–SnO<sub>x</sub>/Al<sub>2</sub>O<sub>3</sub> catalysts with varying Sn/Pt atomic ratios in the range of 0–3.8 in the cellulose reaction and for comparison in the reactions of glucose and fructose. Their structures are characterized by X-ray powder diffraction (XRD), X-ray photoelectron spectroscopy (XPS), transmission electron microscopy (TEM), temperature-programmed reduction in H<sub>2</sub> (H<sub>2</sub>-TPR), Fourier transform infrared (FT-IR) spectroscopy using a CO probe molecule and H<sub>2</sub> chemisorption. These detailed studies lead to our understanding of the SnO<sub>x</sub> modification effects on the structures of the Pt–SnO<sub>x</sub>/Al<sub>2</sub>O<sub>3</sub> catalysts and their hydrogenation activities, and consequently on the polyol distribution in the cellulose reaction.

## 2 Experimental

### Catalyst preparation

Pt/Al<sub>2</sub>O<sub>3</sub> and SnO<sub>x</sub>-modified Pt/Al<sub>2</sub>O<sub>3</sub> (denoted as Pt–SnO<sub>x</sub>/Al<sub>2</sub>O<sub>3</sub>) catalysts with seven different nominal Sn/Pt molar ratios in the range of 0.1–3.8, were prepared by the incipient wetness impregnation of  $\gamma$ -Al<sub>2</sub>O<sub>3</sub> (Alfa Aesar, 208 m<sup>2</sup> g<sup>−1</sup>) with aqueous solutions of H<sub>2</sub>PtCl<sub>6</sub>·6H<sub>2</sub>O (AR, Beijing Chemical), H<sub>2</sub>PtCl<sub>6</sub>·6H<sub>2</sub>O (AR, Beijing Chemical) and SnCl<sub>2</sub>·2H<sub>2</sub>O (AR, Shantou Xilong Chemical), respectively. The impregnated samples were dried at room temperature for about 12 h and then at 383 K overnight. Afterwards, they were calcined in flowing air at 673 K for 4 h, and then reduced in a 1 : 4 H<sub>2</sub>/N<sub>2</sub> flow at 673 K for 4 h. The compositions of these samples were measured by profile spec inductively coupled plasma-atomic emission spectrometry (ICP-AES), showing that they contained 1.88–2.07 wt% Pt and that the Sn/Pt atomic ratios for the Pt–SnO<sub>x</sub>/Al<sub>2</sub>O<sub>3</sub> samples were 0, 0.1, 0.3, 0.5, 1.0, 1.5, 2.1, and 3.8 (Table 1). The Pt–SnO<sub>x</sub>/Al<sub>2</sub>O<sub>3</sub> samples were denoted as Pt–SnO<sub>x</sub>(*m*)/Al<sub>2</sub>O<sub>3</sub>, where the *m* in parentheses represents their measured Sn/Pt atomic ratio. For example, Pt–SnO<sub>x</sub>(0.1)/Al<sub>2</sub>O<sub>3</sub> represents the sample with a Sn/Pt atomic ratio of 0.1.

**Table 1** Pt loading, particle size and dispersion on Pt/Al<sub>2</sub>O<sub>3</sub> and Pt–SnO<sub>x</sub>/Al<sub>2</sub>O<sub>3</sub> with different Sn/Pt ratios in the range of 0.1–3.8

Catalyst	Pt loading <sup>a</sup> /wt%	<i>d</i> <sup>b</sup> /nm	<i>D</i> <sup>c</sup> /%
Pt/Al <sub>2</sub> O <sub>3</sub>	2.07	0.8 ± 0.2	100.0
Pt–SnO <sub>x</sub> (0.1)/Al <sub>2</sub> O <sub>3</sub>	2.07	1.1 ± 0.2	83.6
Pt–SnO <sub>x</sub> (0.3)/Al <sub>2</sub> O <sub>3</sub>	2.04	0.9 ± 0.2	94.4
Pt–SnO <sub>x</sub> (0.5)/Al <sub>2</sub> O <sub>3</sub>	1.92	—	76.1
Pt–SnO <sub>x</sub> (1.0)/Al <sub>2</sub> O <sub>3</sub>	1.88	1.0 ± 0.3	55.9
Pt–SnO <sub>x</sub> (1.5)/Al <sub>2</sub> O <sub>3</sub>	1.98	—	44.9
Pt–SnO <sub>x</sub> (2.1)/Al <sub>2</sub> O <sub>3</sub>	1.88	0.9 ± 0.2	38.5
Pt–SnO <sub>x</sub> (3.8)/Al <sub>2</sub> O <sub>3</sub>	1.90	1.2 ± 0.4	31.8

<sup>a</sup> Measured by ICP. <sup>b</sup> Measured by TEM. <sup>c</sup> Measured by H<sub>2</sub> chemisorption.

ReO<sub>x</sub>, SbO<sub>x</sub> and GaO<sub>x</sub>-modified Pt/Al<sub>2</sub>O<sub>3</sub> catalysts were prepared in the same way using HReO<sub>4</sub> (75–80% aqueous solution, Alfa Aesar), Ga(NO<sub>3</sub>)<sub>3</sub>·xH<sub>2</sub>O (99.9%, Alfa Aesar) and SbCl<sub>3</sub> (AR, Sinopharm Chemical), respectively. They contained 1.98–1.99 wt% Pt, and their Re/Pt, Sb/Pt or Ga/Pt atomic ratios were each 0.3.

In a similar way, SnO<sub>x</sub>/Al<sub>2</sub>O<sub>3</sub> (0.36 wt% Sn) was prepared by the incipient wetness impregnation of Al<sub>2</sub>O<sub>3</sub> with ethanol solutions of SnCl<sub>2</sub>·2H<sub>2</sub>O. SnO<sub>x</sub> (4.87 wt% Sn)/Al<sub>2</sub>O<sub>3</sub> was prepared using tri-*n*-butyltin acetate (AR, Alfa Aesar). Sn(OH)<sub>2</sub> and Sn(OH)<sub>4</sub> were prepared by hydrolysis of aqueous SnCl<sub>2</sub>·2H<sub>2</sub>O and SnCl<sub>4</sub>·5H<sub>2</sub>O (AR, Shantou Xilong Chemical) with stoichiometric NH<sub>3</sub>·2H<sub>2</sub>O (AR, 25%–28%, Beijing Chemical), respectively, followed by washing the precipitates with deionized water until the filtrate was neutral. The precipitates were dried at room temperature under vacuum.

### Catalyst characterization

The contents of Pt, Sn, Re, Sb, and Ga in the catalysts were measured by ICP-AES after they were dissolved in the aqua regia solutions.

XRD patterns were recorded on a Rigaku D/MAX-2400 diffractometer using Cu K $\alpha$  radiation ( $\lambda = 1.5406 \text{ \AA}$ ) operated at 40 kV and 100 mA. The  $2\theta$  angle was scanned in the range of 25–50° at a rate of 4° min<sup>−1</sup>.

XPS studies were conducted on an Axis Ultra spectrometer (Kratos Analytical Ltd.) using monochromatic Al K $\alpha$  radiation at a source power of 15 kV. The binding energies were referenced to the Al 2p peak of the Al<sub>2</sub>O<sub>3</sub> support at 74.5 eV.

TEM images were taken on a FEI Tecnai G2 T20 instrument operated at 300 kV. Samples were prepared by uniformly dispersing in ethanol and then placing onto carbon-coated copper grids. The average sizes of metal particles and their size distributions were determined by measuring more than 300 particles randomly distributed in the images. Energy dispersive X-ray (EDX) analysis was carried out on a Philips Tecnai F30 FEI TEM equipped with an EDX spectrometer operated at 300 kV.

Temperature programmed reduction (TPR) experiments were performed on the TP-5000 flow unit (Tianjin Xianquan) by ramping the temperature from 298 to 1073 K at 10 K min<sup>−1</sup>.

in a 5.02% H<sub>2</sub>/N<sub>2</sub> flow (30 mL min<sup>-1</sup>). Prior to the measurements, the samples were calcined at 673 K in an air flow for 4 h. The amounts of consumed H<sub>2</sub> for the samples were measured by a TCD detector and then estimated by referring to the amount obtained from the CuO reduction.

Hydrogen chemisorption measurements were taken on a Quantachrome instrument (Autosorb-1). Calcined samples were reduced *in situ* at 673 K under a 5.02% H<sub>2</sub>/N<sub>2</sub> flow for 4 h, then out-gassed at 673 K for 6 h and finally cooled to room temperature. The total H<sub>2</sub> chemisorption isotherm was performed at 303 K between 4 and 43 kPa H<sub>2</sub>.

FT-IR spectra for CO adsorption were taken in the wavenumber range 4800–600 cm<sup>-1</sup> at 298 K on a Bruker Tensor 27 spectrometer equipped with a MCT detector with a resolution of 4 cm<sup>-1</sup> by averaging 100 scans per spectrum. The samples were pressed into self-supported thin wafers and placed into a quartz cell with CaF<sub>2</sub> windows. Prior to each measurement, the samples were treated in the cell in a 5.02% H<sub>2</sub>/N<sub>2</sub> flow (40 mL min<sup>-1</sup>) at 673 K for 30 min, followed by evacuation at 673 K for 30 min. Upon cooling to ambient temperature in the vacuum, the background spectra of the samples were recorded. Afterwards, the samples were exposed to *ca.* 4 kPa CO for 10 min, and then evacuated for 30 min at 298 K for taking their spectra. All spectra were obtained as difference spectra by subtracting the background spectra of the samples from the spectra after exposure to CO.

Cellulose (microcrystalline, Alfa Aesar) reactions were carried out in a stainless steel autoclave (100 mL) typically at 473 K and 6 MPa H<sub>2</sub> for 30 min with vigorous stirring at a speed of 800 rpm. In a typical run, 1 g cellulose and 0.4 g catalyst were introduced to the autoclave containing 50 mL H<sub>2</sub>O. Afterwards, the reactor was fully purged with H<sub>2</sub> (>99.999%, Beijing Longhui Jingcheng), pressurized with H<sub>2</sub> to 6.0 MPa and then heated to 473 K which was kept constant during the reaction. After cooling to room temperature in water, the reaction mixture was filtrated and the solids were washed several times with deionized water. The filtrate was diluted with deionized water to 100 mL. The solids including the catalyst and remaining cellulose were washed with acetone three times and then fully dried in an oven at 333 K for 24 h. Cellulose conversions were determined by the change in the weight of cellulose loaded before and after the reactions. The products in the liquid phase (*e.g.* polyols) were analyzed by high-performance liquid chromatography (Shimadzu LC-20A) using Bio-Rad Aminex HPX-87H and HPX-87C columns with an RID detector. The products in the gas phase (*e.g.* methane) were analyzed by gas chromatography (Shimadzu 2010) using a HJ-OV-101 column connected to a FID detector. The product selectivities were reported on a carbon basis.

### 3 Results and discussion

Fig. 1 shows the XPS spectra of the Pt 4d core level for the monometallic Pt/Al<sub>2</sub>O<sub>3</sub> and bimetallic Pt–SnO<sub>x</sub>/Al<sub>2</sub>O<sub>3</sub> catalysts with different Sn/Pt atomic ratios between 0.1–3.8. The Pt 4d

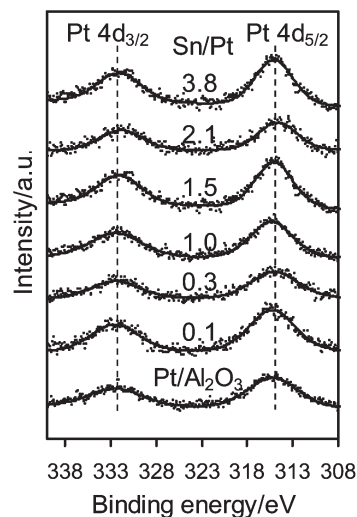


Fig. 1 XPS spectra of Pt 4d for Pt/Al<sub>2</sub>O<sub>3</sub> and Pt–SnO<sub>x</sub>/Al<sub>2</sub>O<sub>3</sub> (~2 wt% Pt) with Sn/Pt atomic ratios in the range of 0.1–3.8.

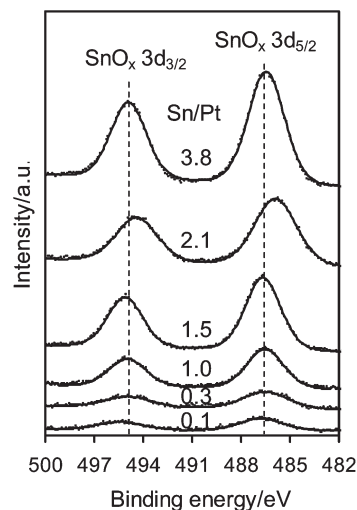
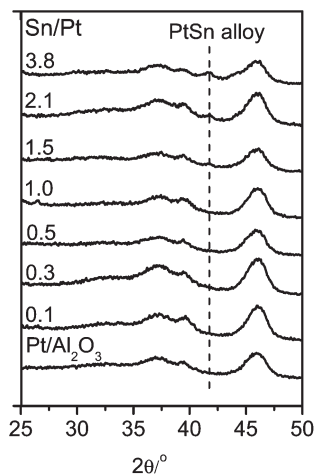


Fig. 2 XPS spectra of Sn 3d for Pt–SnO<sub>x</sub>/Al<sub>2</sub>O<sub>3</sub> (~2 wt% Pt) with Sn/Pt atomic ratios in the range of 0.1–3.8.

lines were analyzed instead of the most intense Pt 4f lines because of their superimposition with the strong Al 2p peak. Only two peaks were observed at binding energies of around 332.5 and 315.0 eV, the characteristic peaks of Pt 4d<sub>3/2</sub> and Pt 4d<sub>5/2</sub> for metallic Pt, respectively, which indicates that the surface Pt species were present as zero-valent Pt in these catalysts.<sup>25,26</sup> In the Sn 3d region, as shown in Fig. 2, the bimetallic Pt–SnO<sub>x</sub>/Al<sub>2</sub>O<sub>3</sub> samples exhibited two symmetrical signals at binding energies of 486.3–487.1 and 494.8–495.6 eV, which can be respectively assigned to Sn3d<sub>5/2</sub> and Sn 3d<sub>3/2</sub> for oxidized tin, Sn<sup>2+</sup> and Sn<sup>4+</sup>, although XPS cannot distinguish between the two oxidation states.<sup>25–27</sup> These results indicate that the SnO<sub>x</sub> species, *i.e.* SnO and/or SnO<sub>2</sub>, were the main Sn species at the surfaces of the bimetallic samples. The SnO<sub>x</sub> species did not reveal XRD peaks (Fig. 3), suggesting that they



**Fig. 3** XRD patterns of Pt/Al<sub>2</sub>O<sub>3</sub> and Pt-SnO<sub>x</sub>/Al<sub>2</sub>O<sub>3</sub> (~2 wt% Pt) with different Sn/Pt atomic ratios in the range of 0.1–3.8.

were highly dispersed. But a diffraction peak at  $2\theta = 41.7^\circ$  appeared when the Sn/Pt molar ratios exceeded 1.5, and the intensity increased with increasing the Sn/Pt ratios (Fig. 3). This peak is tentatively assigned to the Pt–Sn (Sn/Pt atomic ratio = 1 : 1) alloy (JCPDS: 25-0614 and JCPDS: 65-0959), which is confirmed by the representative TEM image for the Sn-rich Pt-SnO<sub>x</sub>(3.8)/Al<sub>2</sub>O<sub>3</sub> catalyst with a Sn/Pt ratio of 3.8, showing a parallel variation of the relative Pt and Sn compositions against the line-scan positions in the energy-dispersive X-ray spectrum (Fig. S1 in the ESI†).<sup>21,28,29</sup> No detection of zero-valent Sn in the XPS spectra (Fig. 2) may be due to the facile surface oxidation of Sn after exposure to air induced by the known strong affinity of tin for oxygen.<sup>30</sup>

The Pt particle sizes for the Pt/Al<sub>2</sub>O<sub>3</sub> and Pt-SnO<sub>x</sub>/Al<sub>2</sub>O<sub>3</sub> samples were characterized by TEM. As shown in Fig. 4 and Fig. S2,† these samples possessed similar Pt particle sizes (0.8–1.2 nm), irrespective of the Sn/Pt ratios. However, their Pt dispersions measured by H<sub>2</sub> chemisorption at 303 K changed with the Sn/Pt ratios (Table 1). An almost 100% Pt dispersion was obtained on Pt/Al<sub>2</sub>O<sub>3</sub>. But the dispersion decreased to ca. 83–94% on the bimetallic samples with the Sn/Pt ratios of 0.1 and 0.3, which then sharply decreased to 31.8% with increasing the Sn/Pt ratio up to 3.8. Such a decrease in the Pt dispersion is obviously not due to the change in the Pt particle sizes, which may arise from the partial blockage of the Pt sites by the SnO<sub>x</sub> species and the formation of the large PtSn alloy crystallites at the higher Sn/Pt ratios.<sup>19,20</sup>

These catalysts were examined in the cellulose reaction. As shown in Table 2, they gave similar cellulose conversions (16.3–22.5%) after 30 min at 473 K and 6 MPa H<sub>2</sub>, reflecting the fact that the cellulose conversions are controlled by the cellulose hydrolysis step that is catalyzed mainly by the H<sup>+</sup> ions generated from hot water under such reaction conditions.<sup>12</sup> However, the selectivities to polyols on these catalysts changed significantly with their Sn/Pt ratios (Table 2). The hexitol selectivity on Pt/Al<sub>2</sub>O<sub>3</sub> was 43.3% (including 34.5% sorbitol, 8.0% mannitol and trace amount of iditol, see Table S1 in ESI†),

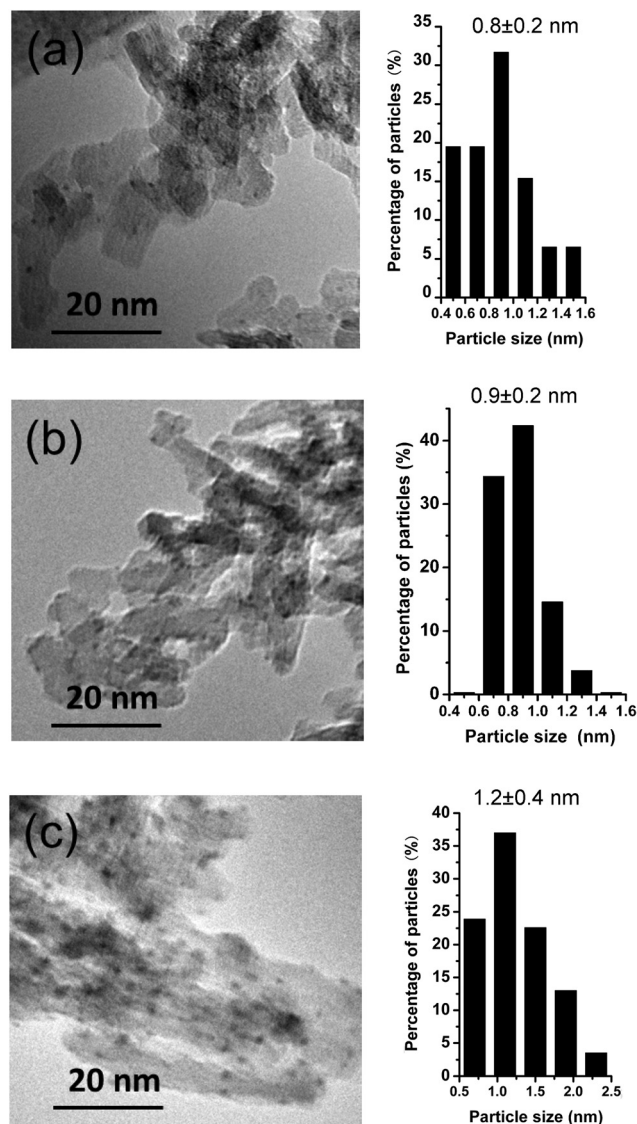


**Fig. 4** TEM images and histograms of Pt particle size distributions of Pt/Al<sub>2</sub>O<sub>3</sub> (a) and Pt-SnO<sub>x</sub>/Al<sub>2</sub>O<sub>3</sub> (~2 wt% Pt) with different Sn/Pt atomic ratios of (b) 0.3, and (c) 3.8.

which is similar to the result (43.0%) reported by Fukuoka and co-workers.<sup>31</sup> The other identified products mainly included pentitols (7.7%), tetrutols (3.4%), glycerol (7.2%), 1,2-propanediol (6.3%), and ethylene glycol (3.5%). Glucose (2.9%), cellobiose alcohol (0.6%) and methane (3.2%) were also detected, which are listed in Table S1 in the ESI† for clarity. The total selectivity of the identified products was 78.1%, not including the unidentified compounds most likely derived from the condensation or degradation of the sugar intermediates. Upon addition of a small amount of SnO<sub>x</sub> to Pt/Al<sub>2</sub>O<sub>3</sub> (Sn/Pt = 0.1), the hexitol selectivity sharply increased from 43.3 to 78.0% while the selectivity to the cracking products, *e.g.* C<sub>2</sub> and C<sub>3</sub> polyols, decreased concurrently from 17.0 to 3.3%. The total selectivity to the identified products reached 96.0%. With increasing the Sn/Pt ratios to 0.3 and 0.5, the hexitol selectivity increased to 81.3 and 82.7%, respectively, nearly twice the

**Table 2** Cellulose conversion and polyol selectivity on Pt/Al<sub>2</sub>O<sub>3</sub> and Pt-SnO<sub>x</sub>/Al<sub>2</sub>O<sub>3</sub> with different Sn/Pt ratios of 0.1–3.8<sup>a</sup>

Catalyst	Conversion%	Selectivity%						
		Hexitols <sup>b</sup> C <sub>6</sub>	Pentitols <sup>c</sup> C <sub>5</sub>	Tetritols <sup>d</sup> C <sub>4</sub>	Glycerol C <sub>3</sub>	1,2-Propanediol C <sub>3</sub>	Acetol C <sub>3</sub>	Ethylene glycol C <sub>2</sub>
Pt/Al <sub>2</sub> O <sub>3</sub>	17.6	43.3	7.7	3.4	7.2	6.3	0.0	3.5
Pt-SnO <sub>x</sub> (0.1)/Al <sub>2</sub> O <sub>3</sub>	16.3	78.0	6.9	1.7	2.2	0.5	0.0	0.6
Pt-SnO <sub>x</sub> (0.3)/Al <sub>2</sub> O <sub>3</sub>	18.9	81.6	5.5	1.3	1.4	0.3	0.0	0.3
Pt-SnO <sub>x</sub> (0.5)/Al <sub>2</sub> O <sub>3</sub>	17.1	82.8	4.1	1.1	1.5	0.3	0.0	0.4
Pt-SnO <sub>x</sub> (1.0)/Al <sub>2</sub> O <sub>3</sub>	17.8	73.4	4.3	3.8	3.2	1.4	0.0	2.9
Pt-SnO <sub>x</sub> (1.5)/Al <sub>2</sub> O <sub>3</sub>	19.6	43.2	2.6	5.2	4.8	5.8	0.0	8.7
Pt-SnO <sub>x</sub> (2.1)/Al <sub>2</sub> O <sub>3</sub>	18.3	3.2	1.6	4.6	3.9	5.6	19.6	17.0
Pt-SnO <sub>x</sub> (3.8)/Al <sub>2</sub> O <sub>3</sub>	22.5	0.8	1.6	1.1	2.0	1.4	25.2	7.4
Pt-SnO <sub>x</sub> (0.3)/Al <sub>2</sub> O <sub>3</sub> + Pt-SnO <sub>x</sub> (3.8)/Al <sub>2</sub> O <sub>3</sub> <sup>e</sup>	23.8	3.9	1.5	2.4	2.4	13.5	12.3	22.0
Pt/Al <sub>2</sub> O <sub>3</sub> + SnO <sub>x</sub> /Al <sub>2</sub> O <sub>3</sub> <sup>f</sup>	19.2	5.7	0.9	2.5	3.2	16.3	14.2	14.2
Pt-ReO <sub>x</sub> (0.3)/Al <sub>2</sub> O <sub>3</sub>	18.0	63.7	14.1	3.2	2.8	1.0	0.0	0.7
Pt-SbO <sub>x</sub> (0.3)/Al <sub>2</sub> O <sub>3</sub>	20.1	51.6	1.6	2.4	7.3	5.6	0.0	2.7
Pt-GaO <sub>x</sub> (0.3)/Al <sub>2</sub> O <sub>3</sub>	17.7	37.1	4.5	2.6	7.5	7.3	0.0	3.3

<sup>a</sup> 1 g cellulose, 0.4 g catalyst, 473 K, 50 mL H<sub>2</sub>O, 6 MPa H<sub>2</sub>, 30 min. <sup>b</sup> Sorbitol, mannitol and iditol. <sup>c</sup> Xylitol and arabitol. <sup>d</sup> Erythritol and threitol. <sup>e</sup> Physical mixture of Pt-SnO<sub>x</sub>(0.3)/Al<sub>2</sub>O<sub>3</sub> and Pt-SnO<sub>x</sub>(3.8)/Al<sub>2</sub>O<sub>3</sub>. <sup>f</sup> Physical mixture of Pt/Al<sub>2</sub>O<sub>3</sub> and SnO<sub>x</sub>/Al<sub>2</sub>O<sub>3</sub>, Sn = 0.36 wt%.

**Table 3** Glucose hydrogenation on Pt/Al<sub>2</sub>O<sub>3</sub> and Pt-SnO<sub>x</sub>/Al<sub>2</sub>O<sub>3</sub> with different Sn/Pt ratios in the range of 0.1–3.8<sup>a</sup>

Sn/Pt	Conversion%	TOF <sup>b</sup> /min <sup>-1</sup>	Selectivity%	
			Hexitols	Fructose
Pt/Al <sub>2</sub> O <sub>3</sub>	35.2	4.6	94.0	1.4
Pt-SnO <sub>x</sub> (0.1)/Al <sub>2</sub> O <sub>3</sub>	43.2	7.1	96.5	0.0
Pt-SnO <sub>x</sub> (0.3)/Al <sub>2</sub> O <sub>3</sub>	50.9	7.4	94.8	0.0
Pt-SnO <sub>x</sub> (0.5)/Al <sub>2</sub> O <sub>3</sub>	63.3	11.4	96.7	0.0
Pt-SnO <sub>x</sub> (1.0)/Al <sub>2</sub> O <sub>3</sub>	38.9	9.6	98.3	0.0
Pt-SnO <sub>x</sub> (1.5)/Al <sub>2</sub> O <sub>3</sub>	25.7	7.6	93.3	4.3
Pt-SnO <sub>x</sub> (2.1)/Al <sub>2</sub> O <sub>3</sub>	6.1	2.2	63.0	30.1
Pt-SnO <sub>x</sub> (3.8)/Al <sub>2</sub> O <sub>3</sub>	3.8	0.3	0.0	82.3

<sup>a</sup> 1 g glucose, 0.4 g catalyst, 393 K, 50 mL H<sub>2</sub>O, 6 MPa H<sub>2</sub>, 10 min.

<sup>b</sup> TOF was calculated from the amount of glucose converted to polyols normalized per exposed Pt atom.

value of Pt/Al<sub>2</sub>O<sub>3</sub>. However, further increasing the Sn/Pt ratios led to a concurrent decline in the hexitol selectivity and an increase in the C<sub>2</sub>–C<sub>5</sub> polyols. Specifically, as the Sn/Pt ratio increased to 2.1, the hexitol selectivity dramatically decreased to as low as 3.2%, whereas the selectivity to the C<sub>2</sub> and C<sub>3</sub> polyols increased to as high as 46.1%. It is noted that acetol, an important chemical intermediate,<sup>32,33</sup> was formed with a selectivity of 19.6%, which further increased to 25.2% by increasing the Sn/Pt ratio from 2.1 to 3.8.

Such a change in the polyol selectivities reflects the effect of SnO<sub>x</sub> on the hydrogenation property of Pt on Al<sub>2</sub>O<sub>3</sub>, as reported previously in many other reactions such as the hydrogenation of crotonaldehyde or citral.<sup>19</sup> This effect is further examined here in the hydrogenation of glucose, the key primary intermediate in the cellulose conversion into polyols. As shown in Table 3, the glucose conversion was 35.2% on Pt/Al<sub>2</sub>O<sub>3</sub> after 10 min at 393 K and 6 MPa H<sub>2</sub>, which increased to 63.3% on Pt-SnO<sub>x</sub>(0.5)/Al<sub>2</sub>O<sub>3</sub> with a Sn/Pt ratio of 0.5, corresponding to

an increase in their turnover frequency (TOF) from 4.6 to 11.4 min<sup>-1</sup> (normalized per exposed surface Pt atom). Afterwards, a further increase in the Sn/Pt ratio up to 3.8 led to a monotonic decline in the glucose conversion and TOF to only 3.8% and 0.3 min<sup>-1</sup>, respectively. The Sn/Pt ratios also influenced the product selectivities in the glucose hydrogenation. Notably, the catalyst with the highest Sn/Pt ratio of 3.8 exhibited essentially no hydrogenation activity, and it catalyzed mainly the glucose isomerization to fructose with a selectivity of 82.3% (at a low conversion of only 3.8%). Clearly, the Pt-SnO<sub>x</sub>/Al<sub>2</sub>O<sub>3</sub> samples with the Sn/Pt ratios of 0.1–1.0 afforded the superior hydrogenation activities, and thus favored the efficient synthesis of hexitols from the hydrogenation of glucose and other C<sub>6</sub> sugar intermediates involved in the cellulose hydrolysis step, which would otherwise undergo degradation or condensation reactions, as observed at the Sn/Pt ratios higher than 1.0 (Table 2). To understand the underlying reason of such SnO<sub>x</sub> effects on the catalytic properties of the Pt-SnO<sub>x</sub>/Al<sub>2</sub>O<sub>3</sub> catalysts, they were characterized by TPR in H<sub>2</sub> (H<sub>2</sub>-TPR) and FT-IR of CO adsorption (CO-IR).

Fig. 5 shows the H<sub>2</sub>-TPR profiles of the Pt-SnO<sub>x</sub>/Al<sub>2</sub>O<sub>3</sub> samples. For comparison, the profiles of Pt/Al<sub>2</sub>O<sub>3</sub> and SnO<sub>x</sub>/Al<sub>2</sub>O<sub>3</sub> are also included. SnO<sub>x</sub>/Al<sub>2</sub>O<sub>3</sub> presents a broad SnO<sub>x</sub> reduction feature around 450 °C, as reported previously.<sup>26</sup> For Pt/Al<sub>2</sub>O<sub>3</sub>, two reduction peaks were observed at 227 and 351 °C.<sup>34,35</sup> The first peak is characteristic of the reduction of the PtO<sub>x</sub> species interacting weakly with the Al<sub>2</sub>O<sub>3</sub> support, while the second one can be assigned to the PtO<sub>x</sub> or oxychlorided Pt species interacting strongly with Al<sub>2</sub>O<sub>3</sub>.<sup>34,35</sup> The total consumption of H<sub>2</sub> corresponds to the stoichiometric reduction of Pt<sup>4+</sup> to Pt<sup>0</sup>. This TPR feature confirms the presence of merely metallic Pt on Pt/Al<sub>2</sub>O<sub>3</sub> after the general treatment with H<sub>2</sub> at 400 °C employed in this work, which is consistent with the XPS result (Fig. 1). Compared to Pt/Al<sub>2</sub>O<sub>3</sub>, an additional peak appeared around 400 °C on the Pt-SnO<sub>x</sub>/

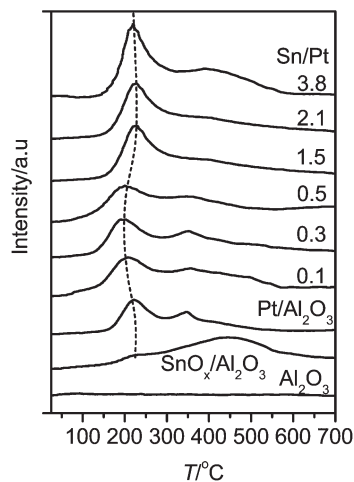


**Fig. 5** TPR profiles of Pt-SnO<sub>x</sub>/Al<sub>2</sub>O<sub>3</sub> with different Sn/Pt atomic ratios in the range of 0.1–3.8, and for comparison Pt/Al<sub>2</sub>O<sub>3</sub>, SnO<sub>x</sub>/Al<sub>2</sub>O<sub>3</sub> (0.36 wt% Sn) and Al<sub>2</sub>O<sub>3</sub>.

Al<sub>2</sub>O<sub>3</sub> catalysts due to the reduction of their SnO<sub>x</sub> species. The PtO<sub>x</sub> reduction peak shifted to lower temperatures around 200 °C with increasing the Sn/Pt ratios to 0.3 and 0.5. It then shifted to the higher temperature around 225 °C, approaching that for Pt/Al<sub>2</sub>O<sub>3</sub>, as the Sn/Pt ratios exceeded 1.0. The higher reducibility of the PtO<sub>x</sub> species observed at the lower Sn/Pt ratios of 0.1–0.5 is related to the strong interaction between PtO<sub>x</sub> and SnO<sub>x</sub>, as reported previously, *via* the electron transfer from SnO<sub>x</sub> to PtO<sub>x</sub> on Pt-SnO<sub>x</sub>/Al<sub>2</sub>O<sub>3</sub>.<sup>36,37</sup> The observed weak effect of SnO<sub>x</sub> on the PtO<sub>x</sub> reduction at the higher Sn/Pt ratios may be due to the partial coverage of the PtO<sub>x</sub> species by SnO<sub>x</sub>, as inferred from the decreased Pt dispersion (Table 1), and the formation of larger PtSn alloy particles with low ability of hydrogen activation.<sup>38</sup> These results are in agreement with those obtained from the *in situ* FT-IR characterization of CO adsorption, as shown below in Fig. 6.

It is known that the SnO<sub>x</sub> surfaces do not significantly adsorb CO.<sup>29,34</sup> Therefore, the CO adsorption bands observed on the bimetallic Pt-SnO<sub>x</sub>/Al<sub>2</sub>O<sub>3</sub> catalysts (Fig. 6) arose from the CO adsorption on the Pt sites. For Pt/Al<sub>2</sub>O<sub>3</sub>, an intense band was detected at 2081 cm<sup>-1</sup>, which corresponds to the linear adsorption of CO on the metallic Pt sites.<sup>34</sup> This band shifted to *ca.* 2073 cm<sup>-1</sup> on the Pt-SnO<sub>x</sub>/Al<sub>2</sub>O<sub>3</sub> samples with Sn/Pt ratios of 0.1–1.0. Such a red-shift on the Pt-SnO<sub>x</sub> catalysts can be explained by the geometric effect of the SnO<sub>x</sub> species that block or dilute the Pt sites, leading to the weakening of dipolar coupling between the adsorbed CO molecules, or by the electronic effect of the SnO<sub>x</sub> species that transfer electrons to the Pt sites, leading to increasing electron back-donation from the d orbitals of Pt to the 2π\* states of CO.<sup>29,39</sup> However, a further increase in the Sn/Pt ratios to over 1.5 led to the appearance of the CO adsorption band at *ca.* 2081 cm<sup>-1</sup>, as observed on Pt/Al<sub>2</sub>O<sub>3</sub>, which excludes the geometric effect of the SnO<sub>x</sub> species. Therefore, the red-shift of the CO adsorption band on the samples with Sn/Pt ratios of 0.1–1.0 is attributed to the electron transfer from SnO<sub>x</sub> to Pt.<sup>37</sup>

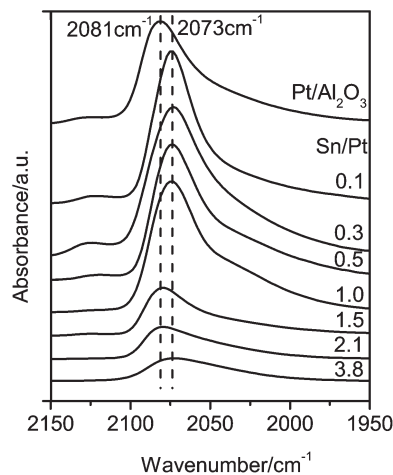
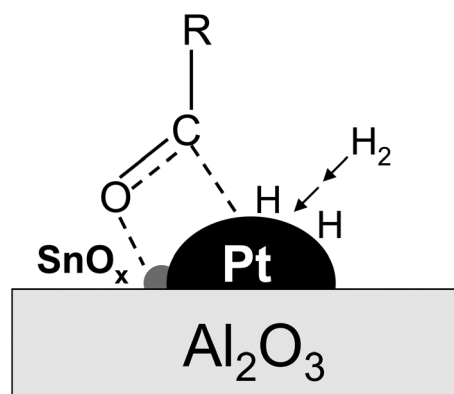


**Fig. 6** FT-IR spectra of CO adsorption on Pt/Al<sub>2</sub>O<sub>3</sub> and Pt-SnO<sub>x</sub>/Al<sub>2</sub>O<sub>3</sub> with Sn/Pt atomic ratios in the range of 0.1–3.8.

It is known that the electron transfer from SnO<sub>x</sub> to Pt can increase the electron density of the Pt sites, and consequently promote H<sub>2</sub> dissociation, required for the hydrogenation of glucose and other C<sub>6</sub> sugar intermediates involved in the cellulose conversion. Moreover, the electron transfer can make the SnO<sub>x</sub> surfaces more positively charged and enhance their Lewis acidity, which, as reported by Gallezot *et al.*, can favor the polarization of the carbonyl group of glucose *via* withdrawing electrons from the oxygen atom in its carbonyl group.<sup>40</sup> Such enhanced polarization then facilitates the C=O hydrogenation by H<sub>2</sub> dissociatively adsorbed on the Pt sites that are in intimate contact with the SnO<sub>x</sub> species, as proposed in Scheme 1. Taken together, these electronic effects of the SnO<sub>x</sub> species led to the superior hydrogenation activities and efficiency for the synthesis of hexitols in the cellulose reaction on the Pt-SnO<sub>x</sub>/Al<sub>2</sub>O<sub>3</sub> catalysts with the Sn/Pt ratios of 0.1–1.0, relative to Pt/Al<sub>2</sub>O<sub>3</sub> (Tables 2 and 3).

Such electronic effects on Pt hydrogenation activity were further confirmed by the Pt/Al<sub>2</sub>O<sub>3</sub> catalysts modified with ReO<sub>x</sub>, SbO<sub>x</sub> and GaO<sub>x</sub> in the cellulose reaction. These catalysts (~2 wt% Pt) possessed similar Pt dispersions (~72–75%) with



**Scheme 1** Schematic description of the promoting role of SnO<sub>x</sub> in glucose hydrogenation on Pt-SnO<sub>x</sub>/Al<sub>2</sub>O<sub>3</sub> catalysts with atomic ratios of 0.1–1.5.

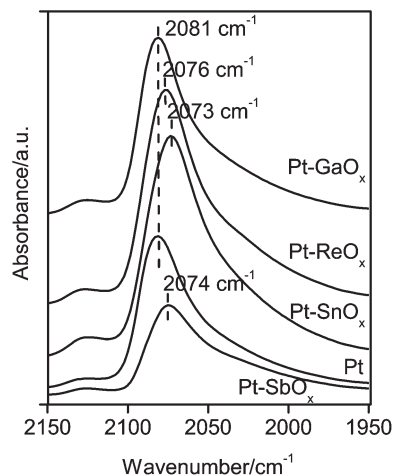


**Fig. 7** FT-IR spectra of CO adsorption on  $\text{ReO}_x$ ,  $\text{SbO}_x$ , and  $\text{GaO}_x$ -modified Pt/ $\text{Al}_2\text{O}_3$  catalysts with atomic ratios of Sb, Re, or Ga to Pt of 0.3, and for comparison, on Pt/ $\text{Al}_2\text{O}_3$  and Pt- $\text{SnO}_x(0.3)/\text{Al}_2\text{O}_3$  with a Sn/Pt atomic ratio of 0.3.

low atomic ratios of Re, Sb or Ga to Pt of 0.3. Their CO-IR spectra show that the CO adsorption band shifted from  $2081\text{ cm}^{-1}$  on Pt/ $\text{Al}_2\text{O}_3$  to  $2076$  and  $2074\text{ cm}^{-1}$  on Pt- $\text{ReO}_x/\text{Al}_2\text{O}_3$  and Pt- $\text{SbO}_x/\text{Al}_2\text{O}_3$ , respectively, while it remained at  $2081\text{ cm}^{-1}$  on Pt- $\text{GaO}_x/\text{Al}_2\text{O}_3$  (Fig. 7). Such different effects on the CO adsorption reflect the electron transfer to Pt from  $\text{ReO}_x$  and  $\text{SbO}_x$ , but not from  $\text{GaO}_x$ , which is consistent with their effects on the Pt hydrogenation activity probed by the cellulose reaction. As shown in Table 2, the selectivity to hexitols increased from 43.3% on Pt/ $\text{Al}_2\text{O}_3$  to 63.7 and 51.6% on Pt- $\text{ReO}_x/\text{Al}_2\text{O}_3$  and Pt- $\text{SbO}_x/\text{Al}_2\text{O}_3$ , respectively, but it was as low as 37.1% on Pt- $\text{GaO}_x/\text{Al}_2\text{O}_3$  at the similar cellulose conversions (17.6–20%). These results reveal that  $\text{ReO}_x$  and  $\text{SbO}_x$ , similar to  $\text{SnO}_x$ , can donate electrons to the Pt sites on  $\text{Al}_2\text{O}_3$ , and accordingly improve their hydrogenation activity.

Next, we examine the underlying basis for the preferential conversion of cellulose to the  $\text{C}_2$  and  $\text{C}_3$  polyols at the expense of hexitols on the Pt- $\text{SnO}_x/\text{Al}_2\text{O}_3$  catalysts with Sn/Pt ratios above 1.5. These catalysts exhibited inferior hydrogenation activity, which appears to lead to the degradation of glucose or other  $\text{C}_6$  sugar intermediates to form the  $\text{C}_2$  and  $\text{C}_3$  products, rather than the sugar hydrogenation to hexitols. However, our control experiments show that the low hydrogenation activity cannot fully account for the formation of the degradation products. For example, as aforementioned, the total selectivity of the  $\text{C}_2$  and  $\text{C}_3$  products was  $\sim 36\%$  on the Pt- $\text{SnO}_x(3.8)/\text{Al}_2\text{O}_3$  catalyst with the Sn/Pt ratio of 3.8 (Table 2). After physically mixing it with the active hydrogenation catalyst of Pt- $\text{SnO}_x(0.3)/\text{Al}_2\text{O}_3$ , the selectivity to hexitols only increased slightly from 0.6 to 3.9%, but the  $\text{C}_2$  and  $\text{C}_3$  polyols were still the dominant products (50.2% selectivity) at similar cellulose conversions (Table 2). This result suggests that the  $\text{SnO}_x$  species not in contact with the Pt sites on Pt- $\text{SnO}_x(3.8)/\text{Al}_2\text{O}_3$  contributes to the cleavage of the C–C bonds in glucose or other sugar intermediates in the cellulose reaction, most likely following the retro-aldol condensation mechanism, to form

**Table 4** Cellulose conversion and polyol selectivity on different  $\text{SnO}_x$  samples<sup>a</sup>

Catalyst	Conversion %	Selectivity/%			
		Glucose	Glycerol	Acetol	Lactic acid
$\text{SnO}$	17.1	5.3	2.6	8.4	2.2
$\text{SnO}_2$	19.9	10.2	2.1	6.5	5.7
$\text{Sn}(\text{OH})_4$	12.0	0.6	1.8	4.7	4.3
$\text{Sn}(\text{OH})_2$	15.5	1.7	5.1	21.1	8.2
$\text{SnO}_x/\text{Al}_2\text{O}_3$ <sup>b</sup>	8.2	12.5	3.6	12.2	13.0
$\text{SnO}_x/\text{Al}_2\text{O}_3$ -recycled <sup>b</sup>	6.8	11.8	3.2	9.9	17.3

<sup>a</sup> 1 g cellulose, 0.4 g catalyst, 473 K, 50 mL  $\text{H}_2\text{O}$ , 6 MPa  $\text{H}_2$ , 30 min.

<sup>b</sup> Sn = 4.87 wt%.

the  $\text{C}_2$  and  $\text{C}_3$  products, which apparently occurs more readily on the  $\text{SnO}_x$  species than the sugar hydrogenation to hexitols on the Pt sites. This proposition was indeed confirmed by the catalytic performance of another physical mixture containing Pt/ $\text{Al}_2\text{O}_3$  and  $\text{SnO}_x/\text{Al}_2\text{O}_3$  (0.36 wt% Sn). As shown in Table 2, the addition of  $\text{SnO}_x/\text{Al}_2\text{O}_3$  to Pt/ $\text{Al}_2\text{O}_3$  even at a low Sn/Pt ratio of 0.3, led to a sharp increase in the selectivity to the  $\text{C}_2$  and  $\text{C}_3$  polyols from 9.8 to 48.8% and a concurrent decline in the selectivity to hexitols from 43.3 to 5.7% at similar cellulose conversions. Such catalytic properties of the  $\text{SnO}_x$  species were more directly evidenced from the cellulose reaction catalyzed only by  $\text{SnO}_x$ , as discussed below.

To understand the nature of the active  $\text{SnO}_x$  species responsible for breaking the C–C bonds, different tin samples including bulk  $\text{SnO}$ ,  $\text{SnO}_2$ ,  $\text{Sn}(\text{OH})_2$  and  $\text{Sn}(\text{OH})_4$  were examined for the cellulose reaction in the absence of the Pt sites (Table 4). On these samples, three  $\text{C}_3$  products: glycerol, acetol and lactic acid, were detected. Other products included glucose and trace amounts of  $\text{C}_2$  compounds (e.g. glycolic acid).  $\text{SnO}$ ,  $\text{SnO}_2$  and  $\text{Sn}(\text{OH})_4$  exhibited low selectivities to glycerol, acetol and lactic acid in the range of 10–15%, which increased significantly to 34.4% on  $\text{Sn}(\text{OH})_2$  at similar cellulose conversions under identical conditions. These results indicate that  $\text{Sn}(\text{OH})_2$  is the active  $\text{SnO}_x$  species for catalyzing the retro-aldol condensation of glucose or other  $\text{C}_6$  sugars to form the  $\text{C}_2$  and  $\text{C}_3$  products in the cellulose reaction. To further understand the catalytic properties of the  $\text{SnO}_x$  species on the Pt- $\text{SnO}_x/\text{Al}_2\text{O}_3$  catalysts,  $\text{SnO}_x/\text{Al}_2\text{O}_3$  (4.87 wt% Sn) was examined. Similar to  $\text{Sn}(\text{OH})_2$ , it catalyzed cellulose conversion to the  $\text{C}_3$  products at a selectivity of 28.8%, which remained essentially unaltered (i.e. 30.4%) when the  $\text{SnO}_x/\text{Al}_2\text{O}_3$  sample was recycled. These results imply that  $\text{Sn}(\text{OH})_2$  species were formed on  $\text{SnO}_x/\text{Al}_2\text{O}_3$  and remained stable during the cellulose reaction.

Furthermore, it is noted that the  $\text{C}_3$  products were dominant over the  $\text{C}_2$  products on the  $\text{SnO}_x$  and Pt- $\text{SnO}_x/\text{Al}_2\text{O}_3$  (with the higher Sn/Pt ratios) catalysts, as shown in Tables 2 and 4. Following the retro-aldol condensation mechanism, glucose tends to convert to the  $\text{C}_2$  products while the  $\text{C}_3$  products dominate in the fructose reaction. Therefore, we suggest that the formation of the  $\text{C}_3$  products in the cellulose reaction involves the isomerization of glucose to fructose prior to its

retro-aldol condensation on the  $\text{SnO}_x$  species, which is consistent with the observed conversion of glucose to fructose, as shown in Table 3, on the Pt– $\text{SnO}_x/\text{Al}_2\text{O}_3$  catalysts with high Sn/Pt ratios of 2.1 and 3.8 at 393 K. This suggestion can account for the formation of the  $\text{C}_3$  products. The retro-aldol condensation of fructose is known to form the glyceraldehyde and dihydroxyacetone intermediates which undergo hydrogenation to glycerol (or further to 1,2-propanediol), or dehydration to pyruvaldehyde. The pyruvaldehyde intermediate then converts to acetol and lactic acid by hydrogenation and benzilic acid rearrangement, respectively.<sup>41</sup> This suggestion is further confirmed by the reactions of glucose and fructose on Pt– $\text{SnO}_x(3.8)/\text{Al}_2\text{O}_3$ , predominantly forming acetol and lactic acid. For example, the yields to acetol and lactic acid were ~40.0 and ~55.0% from glucose and fructose, respectively, at 473 K and 6 MPa  $\text{H}_2$  (at a 100% conversion), in which the yields to acetol were 32.9 and 38.2%. Such high acetol yields, although obtained under non-optimized conditions, show the potential reactivity of the  $\text{SnO}_x$  species for the selective cleavage of the C–C bonds in glucose and fructose to produce acetol, an important bio-platform chemical, which have not been reported before directly from the cellulose reaction.

Moreover, the Pt– $\text{SnO}_x/\text{Al}_2\text{O}_3$  catalysts were stable and recyclable under the reaction conditions in this work. Figs. S3 and S4† show the representative results with Pt– $\text{SnO}_x(3.8)/\text{Al}_2\text{O}_3$  in the glucose reaction at 473 K and 6 MPa  $\text{H}_2$ . No significant decline in the yields of the  $\text{C}_2$  and  $\text{C}_3$  products was observed after five successive cycles (Fig. S3†), which is consistent with the essentially identical XRD patterns for this catalyst (Fig. S4†) before and after the five cycles. This result reveals that the hydrothermal stability of  $\text{Al}_2\text{O}_3$  can be enhanced by loading  $\text{SnO}_x$  on its surface, as is also found with the  $\text{WO}_x/\text{Al}_2\text{O}_3$  catalysts.<sup>5c</sup> In contrast, pure  $\text{Al}_2\text{O}_3$  support readily transformed to  $\text{AlO}(\text{OH})$  in water at 473 K (Fig. S4†).

## 4 Conclusions

The Sn/Pt atomic ratios of  $\text{SnO}_x$ -modified Pt/ $\text{Al}_2\text{O}_3$  catalysts significantly influence their hydrogenation activities and selectivities for cellulose conversion to polyols at 473 K and 6 MPa  $\text{H}_2$ . At lower Sn/Pt ratios of 0.1–1.0, the  $\text{SnO}_x$  species strongly interact with and transfer electrons to the Pt sites, as partly evidenced from the red-shift of the CO adsorption IR bands, leading to the superior hydrogenation activities of the Pt– $\text{SnO}_x/\text{Al}_2\text{O}_3$  catalysts, and thus their higher selectivity to hexitols. The selectivity reaches a maximum of 82.7% at the Sn/Pt ratio of 0.5, which is nearly two times that of Pt/ $\text{Al}_2\text{O}_3$  at similar cellulose conversions (~20%). At higher Sn/Pt ratios than 1.5, the Pt– $\text{SnO}_x/\text{Al}_2\text{O}_3$  catalysts favor the formation of  $\text{C}_2$  and especially  $\text{C}_3$  products (e.g. acetol), as a result of their low hydrogenation activities, and the activity of the segregated  $\text{SnO}_x$  species from the Pt sites, apparently in the form of  $\text{Sn}(\text{OH})_2$ , for cleavage of the C–C bonds of glucose and other  $\text{C}_6$  sugar intermediates in the cellulose reaction, which most likely involves the isomerization of glucose to fructose and its

subsequent retro-aldol condensation on  $\text{SnO}_x$ . Taken together, these results demonstrate the bifunctional role of the  $\text{SnO}_x$  species in tuning the reaction rate of the hydrogenation of glucose and other  $\text{C}_6$  sugar intermediates to hexitols and of their selective degradation to  $\text{C}_2$  and  $\text{C}_3$  products, which is crucial for the rational synthesis of target polyols in the cellulose reaction.

## Acknowledgements

This work was supported by the National Natural Science Foundation of China (20825310, 21173008 and 51121091) and the National Basic Research Project of China (2011CB201400 and 2011CB808700).

## References

- G. W. Huber, S. Iborra and A. Corma, *Chem. Rev.*, 2006, **106**, 4044–4098.
- (a) S. Van de Vyver, J. Geboers, P. A. Jacobs and B. F. Sels, *ChemCatChem*, 2011, **3**, 82–94; (b) J. A. Geboers, S. Van de Vyver, R. Ooms, B. Op de Beeck, P. A. Jacobs and B. F. Sels, *Catal. Sci. Technol.*, 2011, **1**, 714–726.
- A. M. Ruppert, K. Weinberg and R. Palkovits, *Angew. Chem., Int. Ed.*, 2012, **51**, 2564–2602.
- (a) J. C. Serrano-Ruiz and J. A. Dumesic, *Energy Environ. Sci.*, 2011, **4**, 83–99; (b) J. N. Chheda, G. W. Huber and J. A. Dumesic, *Angew. Chem., Int. Ed.*, 2007, **46**, 7164–7183.
- (a) Y. Shen, S. Wang, C. Luo and H. Liu, *Prog. Chem.*, 2007, **19**, 431–436; (b) T. Deng, J. Sun and H. Liu, *Sci. China: Chem.*, 2010, **53**, 1476–1480; (c) Y. Liu, C. Luo and H. Liu, *Angew. Chem., Int. Ed.*, 2012, **51**, 3249–3253.
- J. M. Robinson, C. E. Burgess, M. A. Bently, C. D. Brasher, B. O. Horne, D. M. Lillard, J. M. Macias, H. D. Mandal, S. C. Mills, K. D. O'Hara, J. T. Pon, A. F. Raigoza, E. H. Sanchez and J. S. Villarreal, *Biomass Bioenergy*, 2004, **26**, 473–483.
- H. Kobayashi, H. Ohta and A. Fukuoka, *Catal. Sci. Technol.*, 2012, **2**, 869–883.
- V. I. Sharkov, *Angew. Chem., Int. Ed. Engl.*, 1963, **2**, 405–409.
- R. Palkovits, K. Tajvidi, A. M. Ruppert and J. Procelewska, *Chem. Commun.*, 2011, **47**, 576–578.
- A. Fukuoka and P. L. Dhepe, *Angew. Chem., Int. Ed.*, 2006, **45**, 5161–5163.
- N. Yan, C. Zhao, C. Luo, P. J. Dyson, H. Liu and Y. Kou, *J. Am. Chem. Soc.*, 2006, **128**, 8714–8715.
- C. Luo, S. Wang and H. Liu, *Angew. Chem., Int. Ed.*, 2007, **46**, 7636–7639.
- J. Pang, A. Wang, M. Zheng, Y. Zhang, Y. Huang, X. Chen and T. Zhang, *Green Chem.*, 2012, **14**, 614–617.
- (a) S. Van de Vyver, J. Geboers, W. Schutyser, M. Dusselier, P. Eloy, E. Dornez, J. W. Seo, C. M. Courtin, E. M. Gaigneaux, P. A. Jacobs and B. F. Sels, *ChemSusChem*, 2012, **5**, 1549–1558; (b) J. Geboers, S. Van de Vyver,

- K. Carpentier, P. Jacobs and B. Sels, *Chem. Commun.*, 2011, **47**, 5590–5592; (c) J. Geboers, S. Van de Vyver, K. Carpentier, K. de Blohouse, P. Jacobs and B. Sels, *Chem. Commun.*, 2010, **46**, 3577–3579.
- 15 W. Deng, X. Tan, W. Fang, Q. Zhang and Y. Wang, *Catal. Lett.*, 2009, **133**, 167–174.
- 16 (a) N. Ji, T. Zhang, M. Zheng, A. Wang, H. Wang, X. Wang and J. G. Chen, *Angew. Chem., Int. Ed.*, 2008, **47**, 8510–8513; (b) Y. Zhang, A. Wang and T. Zhang, *Chem. Commun.*, 2010, **46**, 862–864.
- 17 C. L. Pieck, C. R. Vera, C. A. Querini and J. M. Parera, *Appl. Catal., A*, 2005, **278**, 173–180.
- 18 L. Huang, B. Xu, L. Yang and Y. Fan, *Catal. Commun.*, 2008, **9**, 2593–2597.
- 19 I. M. J. Vilella, S. R. de Miguel and O. A. Scelza, *J. Mol. Catal. A: Chem.*, 2008, **284**, 161–171.
- 20 P. D. Zgolicz, V. I. Rodríguez, I. M. J. Vilella, S. R. de Miguel and O. A. Scelza, *Appl. Catal., A*, 2011, **392**, 208–217.
- 21 C. Kappenstein, M. Guerin, K. Lazar, K. Matusek and Z. Paal, *J. Chem. Soc., Faraday Trans.*, 1998, **94**, 2463–2473.
- 22 K. Liberková-Šebková, L. Červený and R. Touroude, *Res. Chem. Intermed.*, 2003, **29**, 609–617.
- 23 A. B. Merlo, V. Vetere, J. F. Ruggera and M. L. Casella, *Catal. Commun.*, 2009, **10**, 1665–1669.
- 24 G. C. Torres, S. D. Ledesma, E. L. Jablonski, S. R. de Miguel and O. A. Scelza, *Catal. Today*, 1999, **48**, 65–72.
- 25 C. Guzmán, G. Del Angel, J. Fierro and V. Bertin, *Top. Catal.*, 2010, **53**, 1142–1144.
- 26 D. L. Hoang, S. A. F. Farrage, J. Radnik, M. M. Pohl, M. Schneider, H. Lieske and A. Martin, *Appl. Catal., A*, 2007, **333**, 67–77.
- 27 Y. Zhou and S. M. Davis, *Catal. Lett.*, 1992, **15**, 51–55.
- 28 N. Kamiuchi, K. Taguchi, T. Matsui, R. Kikuchi and K. Eguchi, *Appl. Catal., B*, 2009, **89**, 65–72.
- 29 G. J. Arteaga, J. A. Anderson, S. M. Becker and C. H. Rochester, *J. Mol. Catal. A: Chem.*, 1999, **145**, 183–201.
- 30 G. Neri, C. Milone, S. Galvagno, A. P. J. Pijpers and J. Schwank, *Appl. Catal., A*, 2002, **227**, 105–115.
- 31 H. Kobayashi, Y. Ito, T. Komanoya, Y. Hosaka, P. L. Dhepe, K. Kasai, K. Hara and A. Fukuoka, *Green Chem.*, 2011, **13**, 326–333.
- 32 S. Niu, Y. Zhu, H. Zheng, W. Zhang and Y. Li, *Chin. J. Catal.*, 2011, **32**, 345–351.
- 33 C. Liu, X. Dou and Y. Lu, *Org. Lett.*, 2011, **13**, 5248–5251.
- 34 V. A. Mazzieri, J. M. Grau, J. C. Yori, C. R. Vera and C. L. Pieck, *Appl. Catal., A*, 2009, **354**, 161–168.
- 35 I. Contreras-Andrade, A. Vázquez-Zavala and T. Viveros, *Energy Fuels*, 2009, **23**, 3835–3841.
- 36 M. Kang, W. Kim, J. Joo, N. Kim, H. Yun and J. Yi, *Catal. Lett.*, 2009, **132**, 417–421.
- 37 F. Somodi, I. Borbáh, M. Hegedus, K. Lázár, E. Sajó István, O. Geszti, S. Rojas, J. L. G. Fierro and J. L. Margitfalvi, *Appl. Surf. Sci.*, 2009, **256**, 726–736.
- 38 R. A. van Santen and M. Neurock, *Molecular Heterogeneous Catalysis*, Wiley, 2006.
- 39 J. Ruiz-Martínez, F. Coloma, A. Sepúveda-Escribano, J. A. Anderson and F. Rodríguez-Reinoso, *Catal. Today*, 2008, **133–135**, 35–41.
- 40 P. Gallezot, P. J. Cerino, B. Blanc, G. Fleche and P. Fuertes, *J. Catal.*, 1994, **146**, 93–102.
- 41 E. P. Maris and R. J. Davis, *J. Catal.*, 2007, **249**, 328–337.